Environmental Science Advances

ROYAL SOCIETY OF CHEMISTRY

PAPER

View Article Online
View Journal | View Issue

Cite this: *Environ. Sci.: Adv.*, 2026, **5**, 78

Uranyl–graphene oxide composite membranes for enhanced photocatalytic tributyl phosphate degradation

Jiahui Ying,[ab] Liqin Huang,[a] Shanshan Yu,[a] Shuang Liu,[c] Zhe Wang,*[a] Jing Chen*[a] and Yuexiang Lu *[a]

Received 14th July 2025
Accepted 5th November 2025

DOI: 10.1039/d5va00207a

rsc.li/esadvances

Tributyl phosphate (TBP), a common reagent in PUREX spent fuel reprocessing, represents a significant organic pollutant and a challenging degradation target. This study leverages the inherent photocatalytic properties of uranyl ions (UO_2^{2+}) for the treatment of radioactive organic waste. A uranyl–graphene oxide (U@GO) composite membrane is facilely fabricated *via* a one-step impregnation method. Comprehensive characterization confirmed uranyl adsorption onto GO, inducing structural and chemical modifications. Systematic photocatalytic evaluation through rhodamine B degradation revealed significantly enhanced performance of the U@GO membrane compared to free-state uranyl ions. Application of the composite membrane to TBP degradation demonstrated excellent photocatalytic efficiency, highlighting the potential of the U@GO membrane for radioactive wastewater treatment. Combined with electron spin resonance and nuclear magnetic resonance characterization, mechanistic investigation identified that uranyl ions coordinated to the GO membrane act as the primary active sites for photocatalysis. Upon light irradiation, the generated reactive oxygen species, as well as the excited uranyl ions, attack TBP to degrade it into small, harmless molecules such as CO_2 and phosphoric acid, achieving complete mineralization. This work presents a novel approach for utilizing depleted uranium in catalytic applications and offers a promising method and material for the efficient degradation of TBP.

Environmental significance

The removal of organic compounds from industrial wastewater, due to their toxicity to both biological systems and the environment, has long been a challenging task. Photocatalysis, with its advantages of high efficiency and environmental friendliness, has been extensively investigated and applied in wastewater treatment. In this study, we developed a uranyl ion-loaded graphene oxide membrane *via* a simple one-step impregnation method, which is easy to recover and reuse while exhibiting photocatalytic degradation performance. Furthermore, the membrane demonstrates photocatalytic degradation capability towards tributyl phosphate (TBP), a common organic pollutant in nuclear industry wastewater. This work presents a strategy for utilizing uranyl ions in photocatalytic degradation of TBP, aligning with the "treat waste with waste" approach, and expands the application scope of heterogeneous photocatalysis involving uranyl ions.

1. Introduction

Depleted uranium, a by-product of nuclear fuel enrichment processes, is predominantly stockpiled as strategic reserves. While historically utilized for military purposes, recent scientific investigations have increasingly explored its potential in civilian applications. Catalysis has emerged as a frontier research domain within uranium chemistry, particularly focusing on uranyl ions (UO_2^{2+}) – the predominant aqueous uranium species. These ions exhibit ligand-to-metal charge transfer (LMCT) under visible light irradiation, generating electronically excited states that undergo quenching through two primary pathways: single electron transfer (SET) with organic substrates or hydrogen atom transfer (HAT) from small molecules. Photoactivated uranyl complexes demonstrate remarkable catalytic versatility, enabling biomolecular cleavage, C–H bond functionalization, pollutant degradation, and photocatalytic hydrogen production, as well as the degradation of plastics (*e.g.*, PVC and PET) and lignin, which have recently attracted significant attention.[1–15] Some excellent reviews further detail uranium complex applications in organic synthesis and small molecule activation.[16–18]

Graphene oxide and its derivatives have emerged as prominent carbon-based nanomaterials in contemporary research. Characterized by their exceptional specific surface area,

[a]*Institute of Nuclear and New Energy Technology, Tsinghua University, Beijing 100084, P. R. China. E-mail: luyuexiang@mail.tsinghua.edu.cn*

[b]*Department of Engineering Physics, Tsinghua University, Beijing 100084, P. R. China*

[c]*Nuclear Research Institute for Future Technology and Policy, Seoul National University, Seoul 08826, Republic of Korea*

abundant surface functional groups, efficient photo-generated electron acceptor capabilities, and versatile solution processability, these materials demonstrate significant potential for enhancing photocatalytic performance through composite formation with various inorganic materials (*e.g.*, ZnO,[19] TiO_2,[20] and Fe_3O_4[21]). Uranyl ions have been successfully incorporated into diverse matrices including zeolites,[22] clay,[23] mesoporous silicon,[24] TiO_2,[25] and other materials. In our previous work, we synthesized highly adsorptive SiO_2 and verified its application in photocatalytic degradation after adsorbing uranyl ions.[26] However, no studies to date have explored GO–uranyl composites for photocatalytic applications. This research gap primarily stems from the predominant focus on investigating the adsorption capacity of GO for uranyl species rather than its photocatalytic synergies.

TBP, a key extractant in nuclear fuel reprocessing *via* the PUREX process, demonstrates notable resistance to chemical degradation. During spent fuel treatment, nitric acid and irradiation generate degradation byproducts such as dibutyl phosphate (DBP), monobutyl phosphate (MBP), and butanol.[27,28] Beyond nuclear applications, TBP serves critical roles in aerospace systems,[29] textile manufacturing, and rare earth extraction processes. However, its effective removal remains a persistent challenge across industrial sectors. Reported degradation strategies include hydrolysis,[30] wet-oxidation,[31] and biological processes.[32] Notably, photocatalytic processes have demonstrated effectiveness in degrading of TBP.[33,34] Currently, there is a scarcity of research on the photocatalytic degradation of TBP.

The application of uranyl is primarily limited by legal restrictions and radioactive concerns, making the photocatalytic degradation of TBP in spent fuel reprocessing wastewater a feasible scenario. In this study, a simple one-step impregnation method is used to adsorb uranyl ions onto graphene oxide, which is subsequently integrated into a membrane. The primary aim is to investigate the photocatalytic properties of uranyl-adsorbed graphene oxide. Various characterization techniques are employed to compare the results with previous studies on the adsorption of uranyl by graphene oxide. Furthermore, the enhanced photoactivity of uranyl ions after incorporation of graphene oxide is verified using RhB. Finally, the composite membrane demonstrates its capability for photocatalytic TBP degradation, validating its practical applicability.

2. Materials and methods

2.1. Materials

$UO_2(NO_3)_2 \cdot 6H_2O$ was obtained from the inventory of the Institute of Nuclear and New Energy Technology, Tsinghua University. NaOH and HNO_3 were purchased from Aladdin. RhB was procured from Hebei Bailingwei Hyperfine Materials Co., Ltd., while TBP was acquired from Beijing Tongguang Reagent. 0.22 μm acetate fibre films were purchased from Shanghai Xingya Reagent Factory. All reagents used were analytically pure and required no further purification steps. The water employed in this study was 18.2 MΩ ultra-pure water obtained from a Merck Milli-Q integral 5 system.

2.2. Fabrication of photocatalytic composite membranes

The synthesis of graphene oxide utilized in this experiment followed the procedure described in our previous work.[35] The synthesized graphene oxide was dispersed in an aqueous solution using ultrasonication and then diluted to a concentration of 0.12 g L^{-1}. Uranyl nitrate solutions were prepared at different concentration gradients (0–1000 ppm). The pH of the uranyl nitrate solution was adjusted to 5 using NaOH and HNO_3, without affecting the concentration of uranyl ions. A mixture containing 5 mL of graphene oxide and 25 mL of uranyl nitrate solution was transferred into a centrifuge tube. After thorough mixing by oscillation, the mixture was further dispersed uniformly through ultrasonic treatment for 15 min, followed by continuous shaking at room temperature for 24 h on a shaker table. Subsequently, the resulting composite materials were extracted and filtered onto acetate fiber membrane substrates using a vacuum filtration device to form membranes, which were labeled as U@GO-*X* (*X* represents the initial uranyl nitrate concentration in ppm). Graphene oxide films that did not contain any uranyl ions were labeled as GO.

2.3. Photocatalytic measurement

2.3.1. RhB degradation experiment. A 10 ppm RhB solution was prepared and 50 mL was used for each photocatalysis experiment. The pH was adjusted to 5 using NaOH and HNO_3, ensuring no impact on the original RhB concentration. A CEAULIGHT CEL-HXF300-T3 light source system (visible light, 100 mW cm^{-2}) was employed as the xenon lamp source. All photocatalytic experiments were conducted under a circulating cooling water system at 298 K. The membranes were introduced into the RhB solution, followed by a dark reaction period of 4 h to achieve complete adsorption before light irradiation commenced. A UV-5200 ultraviolet spectrophotometer from Shanghai Yuan Analysis Instrument was used to measure absorbance by sampling 2 mL every hour. For the TBP photocatalytic degradation experiment, a TBP concentration of 15 ppm with a solution volume of 100 mL was used and pH was adjusted to 5. GC-MS analysis was performed for measuring TBP concentration.

2.3.2. Two-cup experiment and scavenging experiments. The two-cup experiment was performed as follows: initially, U@GO-1000 and regular GO membranes were prepared through extraction and filtration processes. As per previous research conducted by our group, the film underwent reduction at 413 K for 4 hours to ensure complete blocking of uranyl ions and RhB molecules. Subsequently, the setup was assembled in the specified sequence with 100 mL of RhB solution and ultrapure water (pH = 5) added separately into each cup. First, U@GO-1000 was positioned facing the RhB solution and the photocatalytic degradation results were recorded. Then, the positions of the solution were switched, with GO facing towards the RhB and the results were recorded. Following a dark reaction period of 4 hours, light irradiation commenced and

changes in absorbance within the solutions were recorded. In the scavenging experiments, the scavengers were used at a concentration of 5 mmol L^{-1}.

2.4. Characterization

2.4.1. Instruments and characterization. The U@GO-1000 material was utilized for characterization in the experiment. X-Ray Diffraction (XRD) patterns were recorded on a Rigaku Ultima IV X-ray diffractometer with Cu Kα radiation (60 kV). A Thermo Escalab 250Xi LUS X-ray photoelectron spectroscopy system, was used for measuring the X-ray photoelectron spectrum (XPS). The binding energy was calibrated against the C 1s photoelectron peak at 284.6 eV as a reference. Fourier transform infrared spectroscopy (FT-IR) was performed using a Thermo Fisher Scientific Nicolet iZ10 Fourier-transform infrared spectrometer, with a scanning range of 500 cm^{-1} to 4000 cm^{-1}. A ZEISS GeminiSEM 360 scanning electron microscopy (SEM) system and an Oxford AztecOne energy-dispersive X-ray spectroscopy (EDS) system were used to observe the microstructure of the photocatalytic membrane and analyze the surface elements. A Horiba Xplora Plus Raman spectroscopy system with a 532 nm laser light source was used, and the scanning range was set from 800 cm^{-1} to 2000 cm^{-1}. Solid ultraviolet spectroscopy was performed using a Shimadzu UV3600IP UV-visible spectrophotometer, with a measurement range of 200 nm to 800 nm. Additionally, photoluminescence (PL) spectra were acquired using an Edinburgh Company's LP980 system, GO and U@GO-1000 were respectively dispersed in aqueous solution and tested at wavelengths ranging from 400 nm to 800 nm. The electron spin resonance (ESR) spectra were recorded using an X-band EPR spectrometer (JEOL, JES FA-200). The operating parameters were as follows: microwave power = 1.0 mW; central magnetic field = 336 mT; sweep width = ±5 mT; sweep time 100 s; modulation frequency = 100.00 kHz; and time constant = 0.03 s. ICP-MS analysis using an Agilent 8900 ICP-MS triple Quad system was used to ascertain the loading capacity of the composite membrane. Using D_2O as the solvent, the ^{31}P nuclear magnetic resonance (NMR) spectrum was recorded on a QOne Instrument Quantum-I Plus spectrometer (400 MHz).

2.4.2. Measurement of TBP. The GC-MS process is described as follows: a QP2010 analytical instrument manufactured by Shimadzu, Japan was utilized, and an Agilent HP-5 capillary column (30 m × 0.25 mm i.d., 0.25 μm film thickness) was employed. Helium gas with a purity of 99.9999% was used as the carrier gas at a column flow rate of 0.93 mL min^{-1}. A sample volume of 1 μL was injected into the GC system using an autosampler operating at 563 K in split mode with a ratio of 1/30. Initially, the oven temperature was set to 50 K and held for 3 min, followed by a temperature ramp of 20 K min^{-1} up to 543 K, resulting in a total run time of 14 minutes. The transfer line and ion source temperatures were maintained at 523 K throughout the analysis. MS detection operated in electron impact (EI) mode at an energy level of 70 eV. Confirmation of the target peak relied on both retention time and characteristic ion presence assessment. For quantitative testing purposes, selective ion monitoring (SIM) mode was employed utilizing fragment ions at m/z values of both 99 and 155.

3. Results and discussion

3.1. Characterization of composite membranes

In order to perform morphology characterization of the material, SEM and EDX were initially employed to observe the surface of U@GO-1000, as depicted in Fig. 1. From the side view presented in Fig. 1a, it can be observed that even after being pumped and filtered onto the acetate fibre membrane, the material still exhibits a membranous structure with a thickness ranging from 100–200 nm. Contrary to typical graphene oxide membranes characterized by smooth and wrinkled surfaces, a rough yet uniform surface is observed in the front-facing image shown in Fig. 1b. The EDX elemental analysis displayed in Fig. 1c reveals an even distribution of uranium throughout the extracted membrane. These SEM results provide preliminary evidence indicating that upon adsorption of uranyl onto graphene oxide, the original layered lamellar structure is no longer present and is instead replaced by a lumpy structure. For a more accurate depiction of the process of uranyl ion adsorption on graphene oxide, we perform XRD, FT-IR spectroscopy, and other characterization studies (Fig. 2). The bulge observed at approximately 22° in the XRD pattern corresponds to the background signal originating from the acetate membrane substrate employed. Additionally, a characteristic peak at $2\theta = 10.8°$ is indicative of the (002) crystal plane of the GO membrane, enabling calculation of interlayer spacing for this layered GO membrane.[36] After the adsorption of uranyl ions, the characteristic peak exhibits a significant reduction in intensity, indicating the disruption of the original ordered stacking structure of graphene oxide (Fig. 2a). As shown in the Raman spectrum in Fig. 2b, distinct characteristic peaks of graphene oxide are observed at 1357 cm^{-1} (D peak) and 1590 cm^{-1} (G peak). Interestingly, while the positions of these peaks remain unchanged after uranyl ion adsorption, a notable increase in the D/G ratio is observed. This increase in the D/G ratio (from 0.790 to 0.931) suggests an increase in the

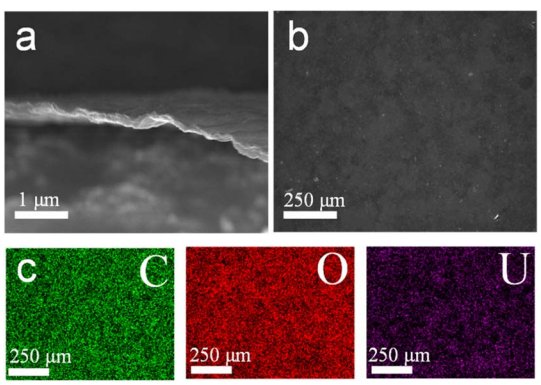

Fig. 1 SEM images of U@GO-1000. (a) The image of U@GO-1000 taken from the side. (b) The image of U@GO-1000 taken from the front side. (c) Energy-dispersive X-ray (EDX) elemental mapping; colour scheme: green for C; red for O; and purple for U.

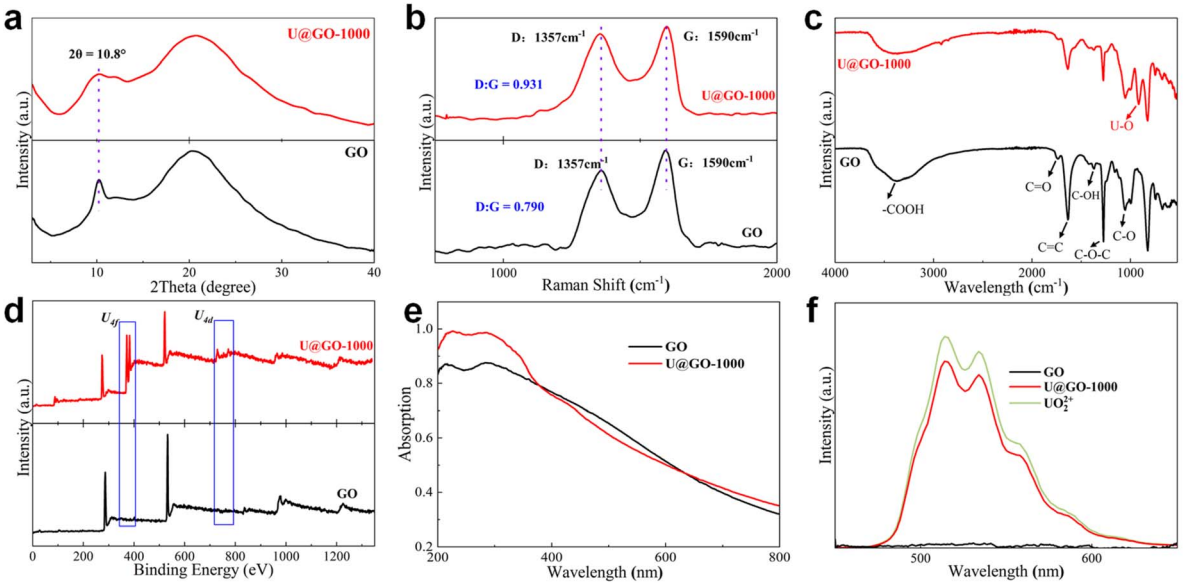

Fig. 2 Characterization of GO and U@GO-1000. (a) XRD patterns, (b) Raman spectrum, (c) FT-IR spectrum, (d) XPS spectrum, (e) UV-Vis spectrum and (f) photoluminescence spectrum.

proportion of defects, structural distortions, and amorphous regions within the carbon framework, disrupting the original crystalline structure. As shown in Fig. 2c, the FT-IR spectrum reveals a new peak at approximately 900 cm^{-1} after uranyl ion adsorption, which is assigned to the asymmetric stretching vibration of the U=O bond in uranyl ions.[22] The peak at around 1373 cm^{-1} corresponds to the O–H bending vibration mode and undergoes a redshift to 1370 cm^{-1} after graphene oxide adsorption. Furthermore, the presence of a peak at 3300 cm^{-1} indicates the involvement of alcohol hydroxyl and carboxyl groups in bending vibrations, with degeneracy occurring upon uranyl ion adsorption.[37]

To gain further insights into the role of graphene oxide and uranyl ions, XPS analysis is conducted on U@GO-1000 and GO. First, upon analyzing the full spectrum in Fig. 2d, a prominent disparity between the two materials is observed: a distinct U 4f characteristic peak at ~400 eV and a U 4d characteristic peak at ~800 eV with considerable intensity. The peaks were deconvoluted based on the O 1s graph (Fig. S1). The distinctive characteristics of the O 1s spectrum result in its relatively broad profile, typically comprising multiple overlapping peaks that combine to form a complex spectral pattern. These peaks interfere with one another and are influenced by water and other contaminants, rendering precise analysis of the O 1s spectrum exceedingly challenging. The GO spectra reveal the presence of a C=O peak at 530.8 eV and a C–O peak at 532.6 eV. The U@GO-1000 spectrum exhibits increased complexity, featuring two peaks corresponding to GO, as well as a distinct peak at 531.2 eV attributed to the uranyl oxygen species (O=U=O) and another at 532.3 eV corresponding to a U–O coordination bond.[38] These findings further substantiate the cooperative bonding between uranyl ions and graphene oxide. Subsequently, the C 1s spectrum was analyzed (Fig. S2). Specifically, peaks were observed at 284.8 eV for C–C/C–C bonds, 286.7 eV for C–OH/C–O–C moieties, 287.6 eV for C=O groups, and finally at 288.8 eV for O=C–OH functionalities. The shift in peak position is not significant, but the change in peak intensity is highly noticeable, particularly for the two peaks at 286.7 eV and 287.6 eV which exhibit a substantial decrease. This observation aligns with findings reported in previous literature.[37] Fig. S3 illustrates the splitting of U 4f peaks into U $4f_{5/2}$ (395.6 eV and 392.7 eV) and U $4f_{7/2}$ (381.9 eV and 385.0 eV). These results confirm that the valence state of uranyl ions remains unchanged during the interaction with GO, indicating their presence as U(VI).

To investigate the optical properties of the material, UV-diffuse reflectance and PL spectroscopy were conducted. The UV-Vis spectrum reveals absorption in both the near-ultraviolet and visible regions. Notably, the visible absorption profile is comparable to that of graphene oxide (GO), while the near-ultraviolet absorption is partially attributed to the transfer of O_2 p orbital electrons from uranium–oxygen bonds to non-bonding or antibonding orbitals of U in uranyl ions[39] (Fig. 2e). The investigation of the charge transfer transition phenomenon holds significant implications for elucidating the mechanism underlying photocatalytic oxidation.[40] PL spectra were recorded at pH 5 (Fig. 2f), where hydrolysis of uranyl ions occurs, resulting in the absence of a single uranyl species in the aqueous solution and leading to degeneracy of the uranyl photoluminescence spectra.[41] Upon addition of GO, a reduction in fluorescence intensity was observed, providing evidence for an interaction between GO and uranyl ions that may impact their photocatalytic performance.

3.2. Photocatalytic performance

The photocatalytic degradation of RhB, a non-biodegradable water contaminant, was conducted to investigate the photocatalytic performance of the U@GO-1000 membrane. It was introduced into the RhB solution, for conducting photocatalytic

reactions. Upon exposure to light, the pink color of the solution diminished while numerous bubbles emerged on the surface of the composite membrane (Fig. 3a). To evaluate the photocatalytic performance of U@GO-1000, the loading capacity of U@GO-1000 was determined to be 2078 mg g^{-1} using ICP-MS analysis and the uranyl ion with an equal adsorption mass (1.2 mg) was subjected to a graphene oxide mass content of 0.6 mg. Subsequently, photocatalytic experiments were performed under identical conditions. The results are presented in Fig. 3b. After 4 hours of photocatalytic degradation, the GO exhibited a degradation rate of 55%, while the uranyl ion and U@GO-1000 demonstrated degradation rates of 48% and 89%, respectively. Meanwhile, no obvious self-degradation of RhB was observed (Fig. S4).

A pseudo-first-order reaction model was employed to fit the reaction rate constant, as depicted in Fig. S5. The fitted k value indicates that the photocatalytic performance of U@GO-1000 surpasses that of the substrate and uranyl ion combination, thereby demonstrating the enhanced photocatalytic activity of uranyl ions after composite graphene oxide incorporation. This observation is consistent with previous findings in mesoporous silicon recombination.[26] Recyclability of catalytic materials is a crucial parameter. Data analysis (Fig. 3c) demonstrates that the composite material retains excellent catalytic performance after five consecutive cycles, with a degradation rate exceeding 82.44%, indicating remarkable recyclability.

The application scenario of photocatalytic TBP degradation holds significant importance, thus necessitating the design and execution of experiments to validate its performance. Consequently, a photocatalytic degradation experiment targeting TBP was conducted, with the outcomes depicted in Fig. 3d. The self-degradation of TBP was rarely observed under pure lighting irradiation (Fig. S6). However, upon the addition of U@GO-1000, the photocatalytic degradation rate increased to 66% within 8 h, demonstrating the photocatalytic degradation capability of U@GO-1000 toward TBP. Additionally, similar bubble formation as observed during RhB degradation was also witnessed in the process of photocatalytic TBP degradation. We deduce these gaseous bubbles to be the final degradation products (CO_2) of RhB and TBP; this suggests a potential common mechanism between the degradation processes of these two distinct organic compounds: uranyl ions combine with graphene oxide and form excited states under light conditions, subsequently reacting with TBP in solution on the surface and degrading it.[40] Using nitrogen gas as a carrier, the bubbles generated during the photocatalytic process were collected *via* the degassing method. Gas chromatography was employed to analyze the collected gases, and significant CO_2 peaks along with trace amounts of O_2 were detected (Fig. S7). This confirms that the final products of the photocatalytic degradation of the two target pollutants are CO_2, consistent with our expectations.

The spent catalysts were characterized, as shown in Fig. S8. The U@GO-1000 retained its membrane structure after use, and no characteristic peaks of graphene oxide are observed. The U 4f XPS spectra revealed that the uranium species dispersed on U@GO-1000 remained in the U(VI) oxidation state, which is different from the results obtained when SiO_2 is used as the substrate.[25] This further indicates that uranyl ions are incorporated into graphene oxide through a coordination interaction and exhibit a certain bonding strength. It also explains the recyclability performance of the composite membrane.

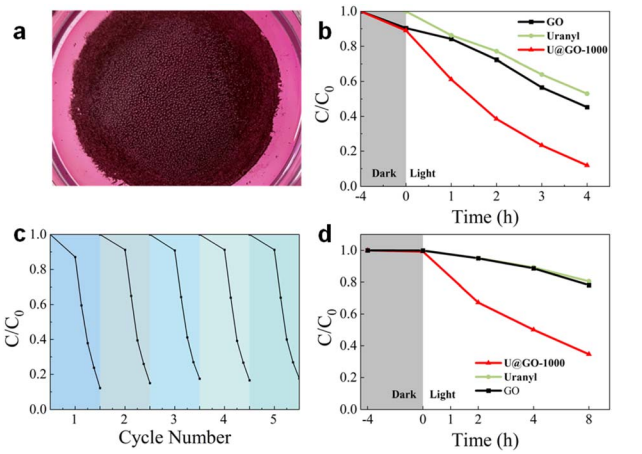

Fig. 3 Photodegradation properties with different membranes. (a) The experimental phenomenon of RhB decomposition by U@GO-1000 under light exposure. (b) Experimental results of photocatalytic degradation of RhB by GO, pure uranyl ions and U@GO-1000. (c) The results of the five-cycle RhB degradation experiment conducted on U@GO-1000. (d) Experimental results of photocatalytic degradation of TBP by the GO membrane, pure uranyl ions and U@GO-1000.

3.3. Mechanism study

Experiments are conducted to investigate the causes of the numerous bubbles observed during the photocatalytic degradation process and to explore the correlation between uranyl ion adsorption capacity and photocatalytic reaction activity. The first experiment was a conditional study, in which the concentration of uranyl ions during immersion adsorption was varied from 50 to 1000 ppm.

The results presented in Fig. S9 were obtained under identical experimental conditions and using the same data processing methods as before. The findings reveal that the photocatalytic performance of the composite exhibits a positive correlation with the concentration of uranyl ions during both immersion and adsorption stages. However, no significant variations in their properties are observed as the uranyl ion concentration changed. For instance, although there exists a two-fold difference in the uranyl ion concentration during the impregnation stage between U@GO-200 and U@GO-400, their photocatalytic degradation characteristics remain comparable. Moreover, when the concentration of uranyl ions during the impregnation stage is only 50 ppm, the performance is comparable to that of substrates without uranyl ions. Based on the findings from conditional and cyclic experiments, it can be inferred that most uranyl ions undergo hydrolysis and adsorption onto the surface of graphene oxide at pH = 5 during the impregnation process, thereby preventing their bonding with graphene oxide. However, some uranyl ions form complexes

with graphene oxide, where the graphene oxide acts as a photoelectron acceptor in photocatalysis processes, ultimately enhancing the photocatalytic performance of uranyl ions.

In order to confirm the surface nature of the photocatalytic reaction, a two-cup experiment is devised employing a customized penetration device (Fig. 4a and S10). However, the degradation performance was reduced due to differences in the effective area size between the membranes used in this experiment and those used previously. Specifically, the pore size of the penetrant cup is 16 mm, which represents only 11.6% of that used in other experiments (where a sand core with a diameter of 47 mm is employed during extraction and filtration stages). Additionally, the amount of RhB solution was doubled. After changing the orientation of the two membranes, no decrease in RhB concentration could be observed as shown in Fig. 4b. This indicates that when the macromolecule RhB is physically isolated by the GO membrane, it does not undergo photodegradation. Experimental observations conducted before and after employing a GO membrane for physical isolation suggest that photodegradation necessitates direct contact between RhB and the U@GO-1000 membrane.

To clarify the photocatalytic degradation mechanism, ESR spectroscopy was performed on U@GO-1000 (Fig. 4c). Distinct signals for hydroxyl radicals (·OH), superoxide radicals ($\cdot O_2^-$), and singlet oxygen ($^1O_2$) were detected under illumination, confirming their active participation in the degradation process. Notably, control experiments with GO showed no detectable radical signals, likely due to insufficient radical generation (Fig. S11). To identify the dominant reactive oxygen species, scavenging experiments were conducted using benzoquinone (BQ, for superoxide radicals $\cdot O_2^-$), EDTA-2Na and TEOA (for holes h^+), TEMP (for singlet oxygen $^1O_2$) and *tert*-butanol (*t*-BuOH, for hydroxyl radicals ·OH). Photodegradation efficiency decreased variably across scavenger treatments, with the most pronounced inhibition observed for hole scavengers (EDTA-2Na and TEOA), followed by weaker suppression with ·OH quenching (Fig. 4d).

To further investigate the mechanism of photocatalytic reactions, we utilized ^{31}P NMR spectroscopy to monitor the intermediate products during the reaction process (Fig. 5a). The ^{31}P NMR spectrum revealed four distinct peaks, which were assigned to MBP (1.95 ppm), DBP (0.98 ppm), phosphoric acid (0.02 ppm), and TBP (−0.12 ppm). The NMR results demonstrate that during the photocatalytic degradation process, the alkyl chains of TBP are targeted and progressively decompose to form DBP, MBP, and phosphate species. These findings are consistent with well-documented observations from previous studies.[34,42] The subsequent oxidative transformation of these alkyl chains leads to the formation of secondary degradation products, primarily lower-molecular-weight organic acids, which are ultimately mineralized into CO_2 through further oxidative processes (Fig. 5b).

Combining all the previous experimental results, the proposed degradation mechanism is illustrated in Fig. 5c. Under visible light irradiation, uranyl ions coordinated with oxygen-containing functional groups on graphene oxide undergo LMCT processes, generating excited-state active UO_2^{2+}. On one hand, the photogenerated electrons from the activated UO_2^{2+} can be separated by the graphene oxide composite, reducing dissolved oxygen in the solution to $\cdot O_2^-$. Subsequently, the remaining holes can further reduce the superoxide anions to $^1O_2$ and ·OH. These reactive oxygen species can directly participate in the degradation process. On the other hand, the activated UO_2^{2+}* can attack the C(sp^3)–H bonds of organic compounds *via* HAT, as has been extensively reported.[8] The reduced photocatalyst can then attack peroxide radicals through a SET process, regenerating its initial state and completing a full catalytic cycle. Throughout this process,

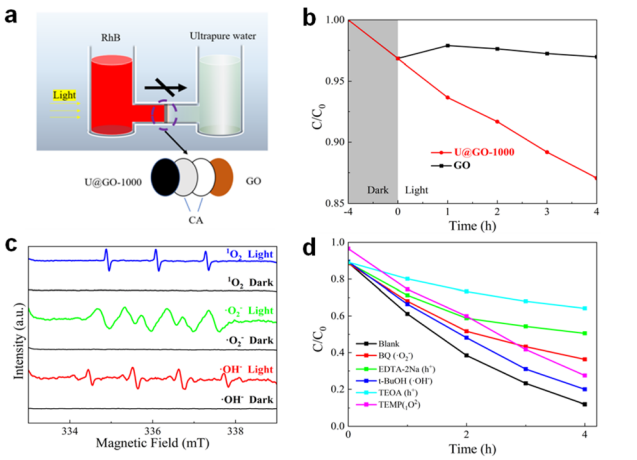

Fig. 4 (a) Schematic diagram of the two-cup experiment. (b) Results of two-cup experiment. (c) ESR spectrum of U@GO-1000; the signals of hydroxyl radicals (•OH), superoxide radicals ($\bullet O_2^-$) and singlet oxygen ($^1O_2$) were measured using free radical scavengers respectively in the dark and under light conditions. (d) Results of scavenging experiments.

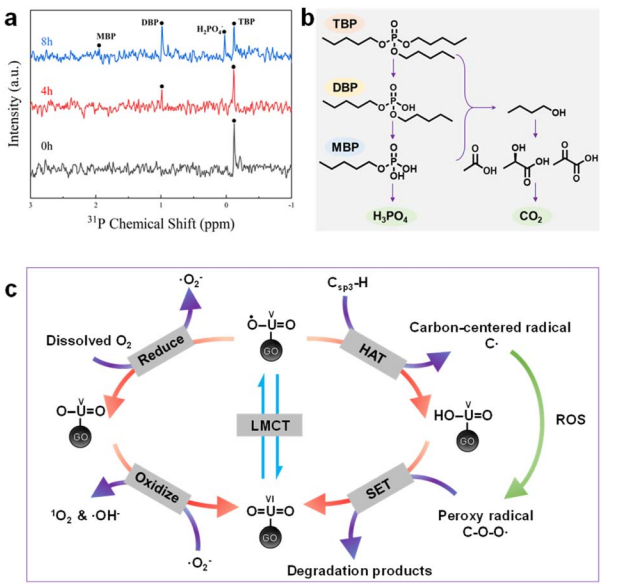

Fig. 5 (a) ^{31}P NMR spectra acquired at different stages of degradation, (b) schematic diagram of photocatalytic degradation of TBP, and the (c) proposed mechanism for the photocatalytic degradation of organic substances by U@GO-1000.

organic compounds are continuously attacked until they are ultimately mineralized into CO_2.

4. Conclusions

In conclusion, we have successfully developed a uranyl-ion functionalized graphene oxide composite membrane (U@GO-1000) *via* a straightforward one-step impregnation method. The composites were thoroughly characterized using analytical techniques, confirming the successful integration of uranyl ions into the GO and the associated structural and chemical modifications. The photocatalytic performance of the composites was evaluated through the degradation of RhB, demonstrating a significant enhancement compared to pure GO or uranyl ions. Moreover, the composite membrane exhibited excellent recyclability, maintaining over 80% degradation efficiency after five consecutive cycles. Notably, U@GO-1000 demonstrated high efficiency in the photocatalytic degradation of radioactive TBP, highlighting its substantial potential for application in treating radioactive TBP waste generated in the PUREX spent nuclear fuel reprocessing cycle. A mechanistic analysis reveals that the specific interaction between uranyl ions and graphene oxide facilitates the generation of highly oxidizing photogenerated holes and a substantial quantity of reactive oxygen species upon illumination. Besides, the excited UO_2^{2+} directly attacks the C–H bonds of organic compounds *via* a hydrogen atom transfer mechanism. This dual-action process continuously dismantles TBP until it is fully converted into harmless small molecules like carbon dioxide (CO_2), achieving complete mineralization. This study offers a new perspective on the utilization of depleted uranium and introduces a novel material and methodology for the photocatalytic degradation of TBP, a challenging organic pollutant in radioactive wastewater. The findings underscore the potential of U@GO-1000 as an efficient and sustainable solution for addressing radioactive wastewater treatment challenges.

Author contributions

Conceptualization: Jiahui Ying, Liqin Huang, Shanshan Yu, Shuang Liu; methodology: Jiahui Ying, Liqin Huang, Shanshan Yu, Shuang Liu; supervision: Zhe Wang, Jing Chen, Yuexiang Lu; writing – original draft: Jiahui Ying; writing – review and editing: Zhe Wang, Jing Chen, Yuexiang Lu. All authors have read and agreed to the published version of the manuscript.

Conflicts of interest

There are no conflicts to declare.

Data availability

The data results are all presented in the paper and can be used if cited.

Supplementary information: supplementary experimental data (such as XPS spectrum) and some of the experimental apparatuses used. See DOI: **https://doi.org/10.1039/d5va00207a**.

Acknowledgements

This work was financially supported by the National Natural Science Foundation of China (Grant No. 22376059, 22422606, U2341289) and sponsored by Beijing Nova Program (No. 20250484900).

Notes and references

1 M. R. Duff Jr and C. V. Kumar, Site-selective photocleavage of proteins by uranyl ions, *Angew Chem. Int. Ed. Engl.*, 2005, **45**, 137–139.
2 J. G. West, T. A. Bedell and E. J. Sorensen, The Uranyl Cation as a Visible-Light Photocatalyst for C(sp(3))-H Fluorination, *Angew Chem. Int. Ed. Engl.*, 2016, **55**, 8923–8927.
3 Q. Zhang, B. Jin, R. Peng, X. Wang, Z. Shi, Q. Liu, S. Lei and H. Liang, Investigation on the Synthesis and Photocatalytic Property of Uranyl Complexes of the β-Diketonates Biscatecholamide Ligand, *Int. J. Photoenergy*, 2017, **2017**, 1–12.
4 K. Takao and S. Tsushima, The oxidation of borohydrides by photoexcited [UO(2)(CO(3))(3)](4-), *Dalton Trans.*, 2018, **47**, 5149–5152.
5 Y. Zhou, D. Hu, D. Li and X. Jiang, Uranyl-Photocatalyzed Hydrolysis of Diaryl Ethers at Ambient Environment for the Directional Degradation of 4-O-5 Lignin, *JACS Au*, 2021, **1**, 1141–1146.
6 J. Meng, Y. Zhou, D. Li and X. Jiang, Degradation of plastic wastes to commercial chemicals and monomers under visible light, *Sci. Bull.*, 2023, **68**, 1522–1530.
7 Y. Meng, D. Liu, Q. Lan, Z. Xie, F. Niu, X. Zhang and Y. Yang, Synthesis, structure, and photocatalytic properties of a two-dimensional uranyl organic framework, *Z. Kristallogr. Cryst. Mater.*, 2023, **238**, 65–71.
8 G. Che, W. Yang, J. Luo, M. Li, X. Li and Q. Pan, Efficient adsorption and photocatalysis over a photorenewable uranyl-organic framework for removal of diquat herbicide, *Sep. Purif. Technol.*, 2024, **334**, 126126.
9 X. Gong, Q. Zhao and C. Zhu, Visible-Light-Initiated Uranyl-Catalyzed Hydrosilylation and Hydrosulfonylation of Alkenes and Alkynes, *Adv. Synth. Catal.*, 2024, **367**, e202400745.
10 X. Wang, J. Li, X. Wei, J. Song, J. Xie, Z. Li, M. Yuan, L. Jiang, Y. Wang, C. Liang and W. Liu, Photocatalytic Hydrogen Peroxide Production by a Mixed Ligand-Functionalized Uranyl–Organic Framework, *ACS Omega*, 2024, **9**, 33671–33678.
11 X. Zhao, L. Bai, J. Li and X. Jiang, Photouranium-Catalyzed C–F Activation Hydroxylation via Water Splitting, *J. Am. Chem. Soc.*, 2024, 11173–11180.
12 B. w. Hu, W. Jin, Z. w. Huang, Z. h. Zhou, K. q. Hu, L. y. Yuan, H. b. He, W. q. Shi and L. Mei, Integrating Uranyl Complexes into Porous Organic Cages for Enhanced Photocatalytic Oxidation of A Mustard-Gas Simulant, *Eur. J. Inorg. Chem.*, 2025, **28**, e202500153.
13 Y. X. Liu, L. Jia, Y. R. Li, P. W. Cai, M. R. Ou, C. Sun and S. T. Zheng, Bridging Uranium Uptake and PET Plastics

Degradation Within an All-Inorganic Polyoxoniobate Framework, *Adv. Funct. Mater.*, 2025, e16939.
14 S.-B. Tang, S.-Y. Zhang, Y.-X. Jiang, Z.-X. Wang, K. Li, Y.-Y. Luo, B. Long and J. Su, Visible-Light-Induced Photocatalytic Degradation of Polyvinyl Chloride under Normal Temperature and Pressure via Uranyl Photocatalyst, *Ind. Eng. Chem. Res.*, 2025, **64**, 7661–7669.
15 L.-Y. Wang, G. Che, Y.-R. Gong, W.-T. Yang, Y. Lin, J.-R. Liu, S.-Y. Chen, M.-D. Xiao, X.-D. Tian and Z.-M. Su, Temperature-driven growth of uranyl-organic frameworks for efficient photocatalytic CO2 reduction, *Inorg. Chem. Front.*, 2025, **12**, 3262–3269.
16 D. R. Hartline and K. Meyer, From Chemical Curiosities and Trophy Molecules to Uranium-Based Catalysis: Developments for Uranium Catalysis as a New Facet in Molecular Uranium Chemistry, *JACS Au*, 2021, **1**, 698–709.
17 N. Behera and S. Sethi, Unprecedented Catalytic Behavior of Uranyl(VI) Compounds in Chemical Reactions, *Eur. J. Inorg. Chem.*, 2020, **2021**, 95–111.
18 A. R. Fox, S. C. Bart, K. Meyer and C. C. Cummins, Towards uranium catalysts, *Nature*, 2008, **455**, 341–349.
19 X. Bai, L. Wang, R. Zong, Y. Lv, Y. Sun and Y. Zhu, Performance enhancement of ZnO photocatalyst via synergic effect of surface oxygen defect and graphene hybridization, *Langmuir*, 2013, **29**, 3097–3105.
20 Y. Liu, Z. Yu, Y. Peng, L. Shao, X. Li and H. Zeng, A novel photocatalytic self-cleaning TiO2 nanorods inserted graphene oxide-based nanofiltration membrane, *Chem. Phys. Lett.*, 2020, **749**, 137424.
21 T. Peik-See, A. Pandikumar, L. H. Ngee, H. N. Ming and C. C. Hua, Magnetically separable reduced graphene oxide/iron oxide nanocomposite materials for environmental remediation, *Catal. Sci. Technol.*, 2014, **4**, 4396–4405.
22 K. Vidya, S. Dapurkar, P. Selvam, S. Badamali and N. Gupta, The entrapment of UO22+ in mesoporous MCM-41 and MCM-48 molecular sieves, *Microporous Mesoporous Mater.*, 2001, **50**, 173–179.
23 S. L. Suib and K. A. Carrado, Uranyl clay photocatalysts, *Inorg. Chem.*, 1985, **24**, 863–867.
24 J. A. Nieweg, K. Lemma, B. G. Trewyn, V. S.-Y. Lin and A. Bakac, Mesoporous silica-supported uranyl: synthesis and photoreactivity, *Inorg. Chem.*, 2005, **44**, 5641–5648.
25 D. S. Selishchev, T. N. Filippov, M. N. Lyulyukin and D. V. Kozlov, Uranyl-modified TiO2 for complete photocatalytic oxidation of volatile organic compounds under UV and visible light, *Chem. Eng. J.*, 2019, **370**, 1440–1449.
26 L. Zheng, N. Zhao, L. Zhang, S. Liu, Z. Wang, X. Wang and Y. Lu, Treating waste with waste: Facile preparation of uranyl based photocatalyst for efficient degradation of organic dyes, *J. Environ. Chem. Eng.*, 2024, **12**, 113297.
27 T. F. Williams, R. W. Wilkinson and T. Rigg, Radiolysis of Tri-n-butyl Phosphate, *Nature*, 1957, **179**, 540.
28 J. G. Burr, The Radiolysis of Tributyl Phosphate, *Radiat. Res.*, 1958, **8**, 214–221.
29 X. Ouyang, B. Fan, H. Yang and R. Qing, Research on Air Content Estimation of Tributyl Phosphate Hydraulic Fluids: A Novel Approach Based on the Vacuum Method, *J. Dyn. Syst. Meas. Contr.*, 2014, **136**, 024503.
30 T. P. Valsala, M. S. Sonavane, S. G. Kore, N. L. Sonar, V. De, Y. Raghavendra, S. Chattopadyaya, U. Dani, Y. Kulkarni and R. D. Changrani, Treatment of low level radioactive liquid waste containing appreciable concentration of TBP degraded products, *J. Hazard. Mater.*, 2011, **196**, 22–28.
31 H. Aly, Wet-oxidation of spent organic waste tributyl phosphate/diluents, *J. Radioanal. Nucl. Chem.*, 2001, **249**, 643–647.
32 S. S. Rangu, B. Muralidharan, S. C. Tripathi and S. K. Apte, Tributyl phosphate biodegradation to butanol and phosphate and utilization by a novel bacterial isolate, Sphingobium sp. strain RSMS, *Appl. Microbiol. Biotechnol.*, 2014, **98**, 2289–2296.
33 M. J. Watts and K. G. Linden, Photooxidation and subsequent biodegradability of recalcitrant tri-alkyl phosphates TCEP and TBP in water, *Water Res.*, 2008, **42**, 4949–4954.
34 E. Drinks, C. Lepeytre, C. Lorentz, M. Dunand, S. Mangematin, F. Dappozze and C. Guillard, UV-a photocatalytic degradation of the radionuclide complexants tributylphosphate and dibutylphosphate, *Chem. Eng. J.*, 2018, **352**, 143–150.
35 Z. Wang, L. Huang, X. Dong, T. Wu, Q. Qing, J. Chen, Y. Lu and C. Xu, Ion sieving in graphene oxide membrane enables efficient actinides/lanthanides separation, *Nat. Commun.*, 2023, **14**, 261.
36 D. Zhao, L. Chen, M. Xu, S. Feng, Y. Ding, M. Wakeel, N. S. Alharbi and C. Chen, Amino Siloxane Oligomer Modified Graphene Oxide Composite for the Efficient Capture of U(VI) and Eu(III) from Aqueous Solution, *ACS Sustainable Chem. Eng.*, 2017, **5**, 10290–10297.
37 S. Song, K. Wang, Y. Zhang, Y. Wang, C. Zhang, X. Wang, R. Zhang, J. Chen, T. Wen and X. Wang, Self-assembly of graphene oxide/PEDOT:PSS nanocomposite as a novel adsorbent for uranium immobilization from wastewater, *Environ. Pollut.*, 2019, **250**, 196–205.
38 M. Schindler, F. C. Hawthorne, M. S. Freund and P. C. Burns, XPS spectra of uranyl minerals and synthetic uranyl compounds. II: The O 1s spectrum, Geochim, *Cosmochim. Acta*, 2009, **73**, 2488–2509.
39 V. A. Volkovich, T. R. Griffiths, D. J. Fray and R. C. Thied, The electronic spectra of alkali metal uranates and band assignments: an analysis of their diffuse reflectance spectra, *Phys. Chem. Chem. Phys.*, 2001, **3**, 5182–5191.
40 Z. T. Yu, Z. L. Liao, Y. S. Jiang, G. H. Li and J. S. Chen, Water-insoluble Ag-U-organic assemblies with photocatalytic activity, *Chemistry*, 2005, **11**, 2642–2650.
41 M. E. D. G. Azenha, H. D. Burrows, S. J. Formosinho, M. G. M. Miguel, A. P. Daramanyan and I. V. Khudyakov, On the uranyl ion luminescence in aqueous solutions, *J. Lumin.*, 1991, **48–49**, 522–526.
42 T. D'Halluin, C. Lepeytre, A. Leydier and C. Julcour, Degradation mechanism of tributyl phosphate by UV/H(2)O(2) treatment and parameters optimization towards the design of a pilot reactor, *Environ. Technol.*, 2021, **42**, 4247–4259.